ISSN: 2579-5821 (Print)
ISSN: 2579-5546 (Online)
URL address: http://journal.unhas.ac.id/index.php/geocelebes
DOI: 10.70561/geocelebes.v9i1.34399

Jurnal Geocelebes Vol. 9 No. 1, April 2025, 43 – 58

# Predicting the Distribution of $CO_2$ Impurities in Hydrocarbons: Seismic Reservoir Characterization in the Northern South Sumatera Basin

Ricky Rahmawati[1], Wahidah[1]*, M. Noor Alamsyah[2], Dadan Hamdani[1], Andi Alamsyah[1]

[1]Geofisika, Universitas Mulawarman, Samarinda 75123, Indonesia.
[2]Geofisika, PetroChina International Jabung, DKI Jakarta 12940, Indonesia.

*Corresponding author. Email: wahidah@fmipa.unmul.ac.id

Manuscript received: 31 March 2024; Received in revised form: 14 April 2025; Accepted: 25 April 2025

**Abstract**

An oil and gas field containing less than 50% carbon dioxide ($CO_2$) impurities is considered economically viable. This study focuses on the 'X' area, located in the northern part of the South Sumatra Basin, and evaluates the sensitivity of elastic parameters—specifically P-impedance and Vp/Vs ratio—to hydrocarbon presence. Additionally, the study assesses the distribution of sandstone reservoirs within the Lower Talang Akar Formation (LTAF) using seismic reservoir characterization methods, while also analyzing the spatial correlation of natural $CO_2$ impurities. Using data from 11 wells equipped with S-wave logs, a multi-attribute analysis was applied to predict reservoir properties in 57 additional wells. Sensitivity analysis of hydrocarbons, reservoir, and non-reservoir zones was then conducted using elastic log parameters. Seismic attributes such as variance and ant tracking were utilized to detect fault patterns and potential fractures. Moreover, Relative Acoustic Impedance maps—based on negative and minimum amplitude summations—were generated to visualize sandstone reservoir distribution and $CO_2$ impurity saturation derived from well tests. Results show that hydrocarbons exhibit greater sensitivity to the Vp/Vs ratio than to P-impedance, although sandstone reservoirs generally display low P-impedance values. Faults in the LTAF surface trend north-south, northwest-southeast, and northeast-southwest, with the highest density in the eastern region of area 'X'. Thick sandstone reservoirs are predominantly found in the northern, southern, western, and southeastern sectors. $CO_2$ saturation trends decrease westward, aligning with reservoir presence and fracture intensity. Zones with thick reservoirs and low $CO_2$ levels are identified as key targets for future exploration and development.

**Keywords**: Multiatribute; P-impedance; Seismic Attributes; South Sumatera Basin; Vp/Vs ratio.

**Citation**: Rahmawati, R., Wahidah, W., Alamsyah, M. N., Hamdani, D., & Alamsyah, A. (2025). Predicting The Distribution of $CO_2$ Impurities in Hydrocarbons: Seismic Reservoir Characterization in the Northern South Sumatera Basin. *Jurnal Geocelebes* 9(1):43–58, doi: 10.70561/geocelebes.v9i1.34399

## Introduction

Hydrocarbons from well drilling typically contain impurities, one of which is carbon dioxide ($CO_2$). These impurities affect the economic viability of an oil and gas field (Hidayat et al., 2020). Sembiring et al. (2019) explain that high $CO_2$ content reduces hydrocarbons' quality and calorific value and that Indonesian gas wells often exhibit very high $CO_2$ concentrations in natural gas. Variations in $CO_2$ saturation levels within hydrocarbon gases have been documented across the South Sumatra Basin (Alamsyah et al., 2023). Fields with $CO_2$ impurity levels exceeding 50% are often reconsidered or even discontinued for further development.

The 'X' area, situated in the northern part of the South Sumatra Basin (Figure 1), produces gas saturated with $CO_2$. Over 60 wells have been drilled to date, penetrating the main producing reservoir, a $CO_2$-saturated gas sandstone reservoir located within the Lower Talang Akar Formation (LTAF). The syn-rift LTAF reservoir, deposited during the initial basin development phase, consists of alluvial and fluvial deposits that transitioned to deltaic

deposits due to transgression (Figure 2-rigth). The sediment model, reservoir characteristics, and geometry of the LTAF (Figure 2-left) are influenced by fault movement, distribution patterns, and basin slope.

Reservoir characterization, a crucial aspect in understanding reservoir properties and detecting its distribution (Ambarsari et al., 2020), is a key player in field development. This study focuses on identifying rock elasticity parameters, P-impedance, and Vp/Vs ratio, which are sensitive in identifying hydrocarbons, reservoirs, and non-reservoirs. It also aims to qualitatively assess fault and fracture distribution and intensity using seismic data, determine reservoir distribution qualitatively integrated with $CO_2$ impurity distribution, and identify economically viable prospective areas for further development.

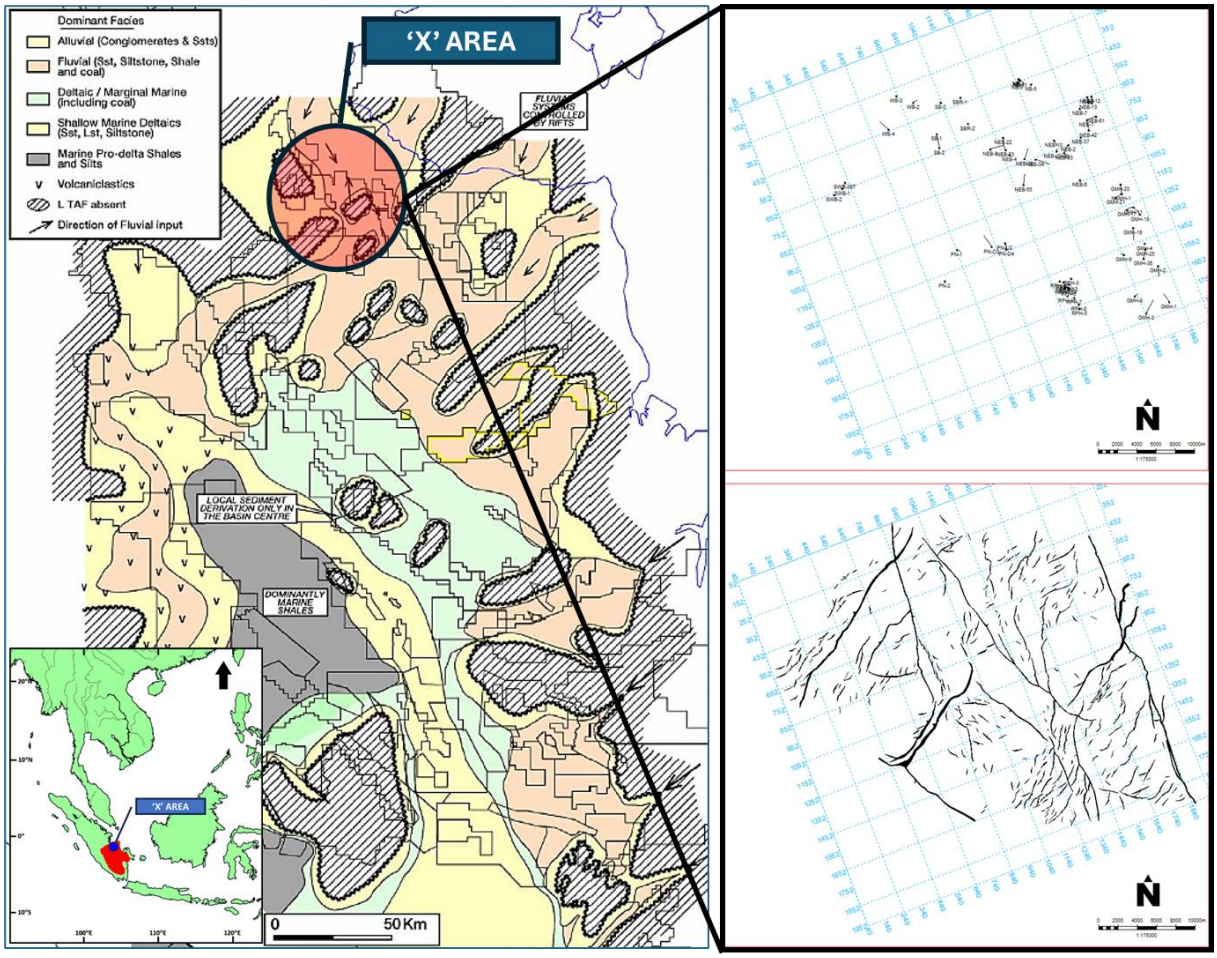


**Figure 1.** The 'X' area, situated in the northern part of the South Sumatra Basin overlaid with paleogeography of LTAF (Modified from Ginger & Fielding, 2005). Left, 3D Seismic Basemap with well location and fault configuration on LTAF, X Area

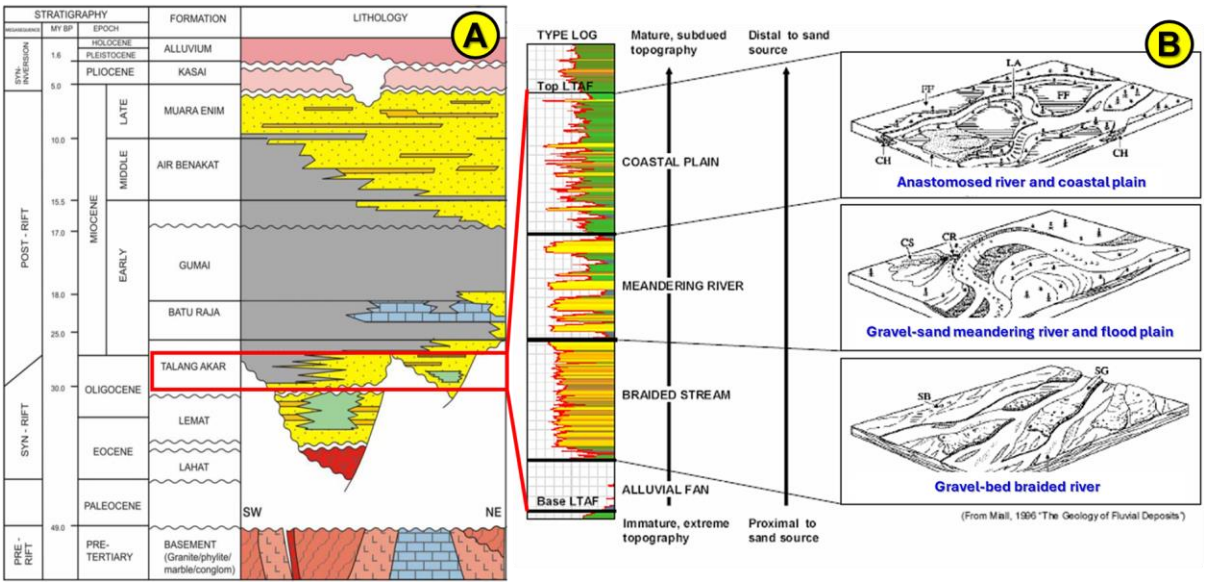


**Figure 2.** (A) South Sumatra Basin generalized structural and stratigraphy section. (B) The sediment model, reservoir characteristics, and geometry of the LTAF from Log Data (Modified from Ginger & Fielding, 2005).

## Materials and Methods

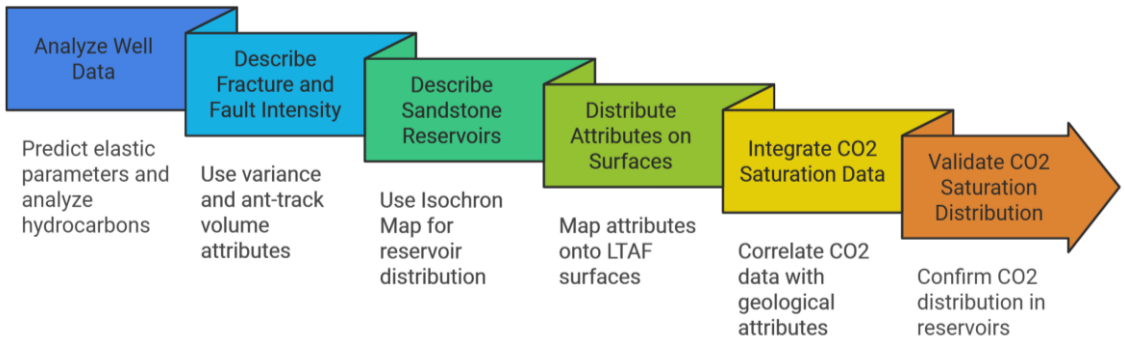


**Figure 3**. Study sequence to validate the distribution of $CO_2$ saturation in the sandstone reservoirs of the LTAF.

The data used in this study are well data and 3D post-stack seismic and the results of LTAF and Basement structure interpretation. Figure 3 shows the first stage of this study is the analysis of well data in the form of prediction of elastic parameters S-Wave by multi attribute method and sensitivity analysis of hydrocarbons, reservoirs, and non-reservoirs using elastic parameters P-Impedance, Vp/Vs ratio. The next stage is the description of fracture and fault intensity using variance and ant-track volume attributes. The results of these volume attributes are distributed on the LTAF and basement surfaces. The distribution of sandstone reservoirs in the LTAF interval is described with the Isochron Map, the sum of negative amplitude and relative impedance degenerate attributes from the LTAF-Basement interval analysis window. Finally, integrating $CO_2$ saturation distribution from well data qualitatively with fracture and fault intensity distribution and sandstone reservoir distribution represents the LTAF interval. This integration is essential to validate the distribution of $CO_2$ saturation in the sandstone reservoirs of the LTAF so that we can predict its origin, saturation, and distribution.

*Multiatribute analysis for S-Wave Log prediction*

Multiattribute analysis is performed with multiattribute linear regression which aims to find an operator in predicting well logs. Validation is a parameter to determine the correctness of the number of attributes used (Pratama et al., 2019). The target log is modeled by a linear equation (Pratama et al., 2019):

$$L\,(t) = w_0 + w_1A_1(t) + w_2A_2(t) + w_3A_3(t) \quad (1)$$

where, $L$ represents the target log and $w_n$ represents the number of log weights and represents the attributes.

The weights in this equation are generated by minimizing the mean-square prediction error (Pratama et al., 2019):

$$E^2 = \sum_{i=1}^{N}(L_i - w_0 - w_1A_{1i} - w_2A_{2i} - w_3A_{3i})^2 \quad (2)$$

where $E$ represents the error, i represents the i-th well and $N$ is the number of known points (i.e. samples) in the analysis.

The validation error for each number of attributes is always greater than the training error due to deleting data (when having one well that lacks log completeness is used). When plotting the average error against the number of attributes used, the training process shows a continuous decrease. However, the validation process often shows a minimum number, and then increases again. This minimum number is the ideal number of attributes to use, and more attributes only cause overtraining. (Pratama, et al., 2019).

*Sensitivity analysis*

Log derivative is a step before conducting sensitivity analysis by cross plotting log P-Impedance and Vp/Vs ratio. The logs used are gamma ray logs to distinguish non reservoir zones and sandstone reservoirs, resistivity logs to distinguish non reservoir zones and fluid-filled reservoirs, and Poisson's ratio logs to discriminate the type of fluid filling the reservoir. The derived logs are made following the equation (Russell, 2017).

$$Ip = Vp \times \rho \quad (3)$$

$$\sigma = \frac{GR - GR_{ss}}{GR_{shale} - GR_{ss}} \times (\sigma_{shale} - \sigma_{ss}) + \sigma_{ss} \quad (4)$$

$$\text{Vp/Vs Ratio} = log\ Vp \times log\ Vs \quad (5)$$

where,

$Ip$ : P-Impedance ((ft/s)*(g/cc))
$Vp$ : P-Wave Velocity (ft/s)
$Vs$ : S-Wave Velocity (ft/s)
$\rho$ : Density (g/cc)
$GR_{Bss}$ : Baseline sand (American Petroleum Institute or API)
$GR_{BShale}$: Baseline shale (American Petroleum Institute or API)
$\sigma_{Bss}$ : Poisson's value of sandstone (unitless)
$\sigma_{BShale}$ : Poisson's value of shale (unitless)

Rock physics analysis is conducted to understand the character and physical properties of rocks and fluids using well data, seismic data, or both. Russell (2015) cross plotted the P-impedance parameter with the Vp/Vs ratio to separate lithologies and fluids into five clusters: shale, wet sand, gas sand, and cemented sand with reference to the rock physics template shown in Figure 4.

There is a contrast in Poisson's ratio in porous rock layers that contain fluid (especially gas), and the Vp value also decreases (Figure 5). So, Poisson's ratio can be used in identifying the presence of gas.

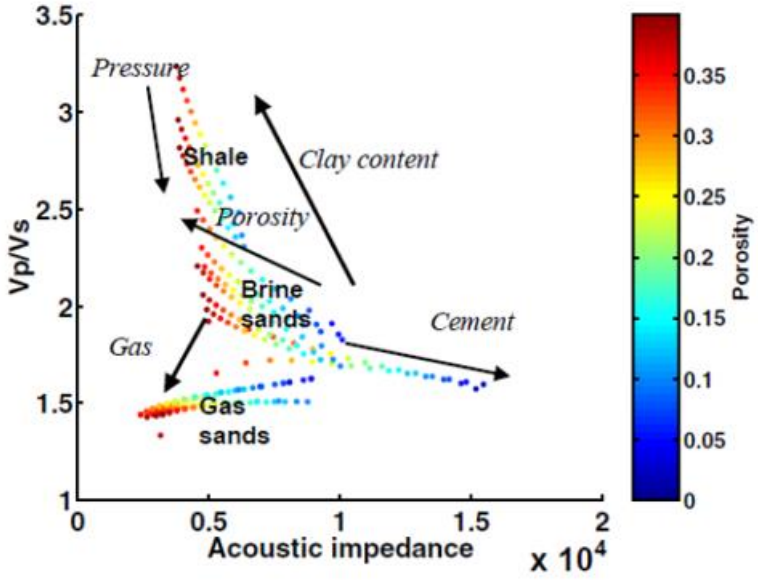


**Figure 4.** Rock physics template (Russell, 2015).

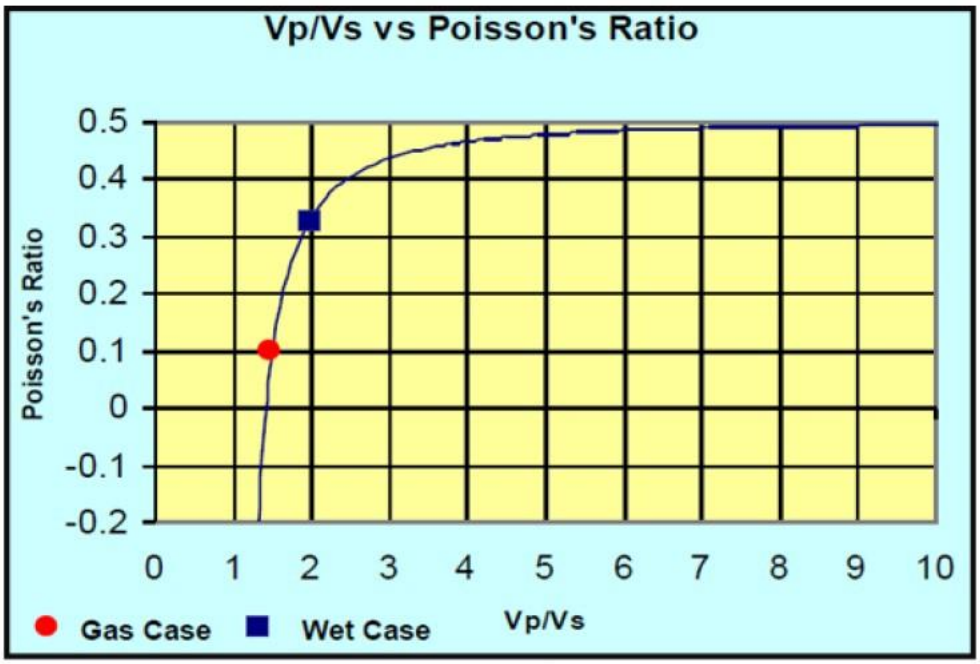


**Figure 5.** Plot Vp/Vs ratio vs Poisson's ratio (Alamsyah & Muhtar, 2017).

*Seismic attributes*

The types of amplitude attributes used in seismic attribute analysis in this study are as follows;

a. Variance Attribute

The variance attribute is called edge detection because it serves to clarify the edge of a surface change. This attribute detects slope changes in seismic data by comparing some data around the main data (Hijria & Danusaputro, 2016). Mathematically, the calculation of Variance normalization is as follows:

$$Variance = \frac{1}{J-1}\sum_{j=1}^{J}(Uji - < Uj >)^2 \quad (6)$$

where, J showing the center trace. <Uj> the mean value of the test and i is the analysis window. This attribute parameter is on the difference in waveforms or traces that are measured based on similarities both

adjacent and vertically. So, it is very effective in describing the boundaries or edges of the main fault zones and fractures (Hijria & Danusaputro, 2016).

b. Ant Tracking Attribute

Variance and ant-track attribute volumes can describe amplitude discontinuities so that they are good at delineating fault structures, fractures, and reservoir bodies in a region (Ngeri et al., 2015; Hijria & Danusaputro, 2016; Abdel-Fattah et al., 2020; Alamsyah et al., 2023). The scattering map obtained is a representation of the intensity of the amplitude discontinuity pattern identified with a darker color, bright red or bright blue. This intensity can be interpreted as the intensity of fractures and faults that we believe are seismically visible (Figure 6).

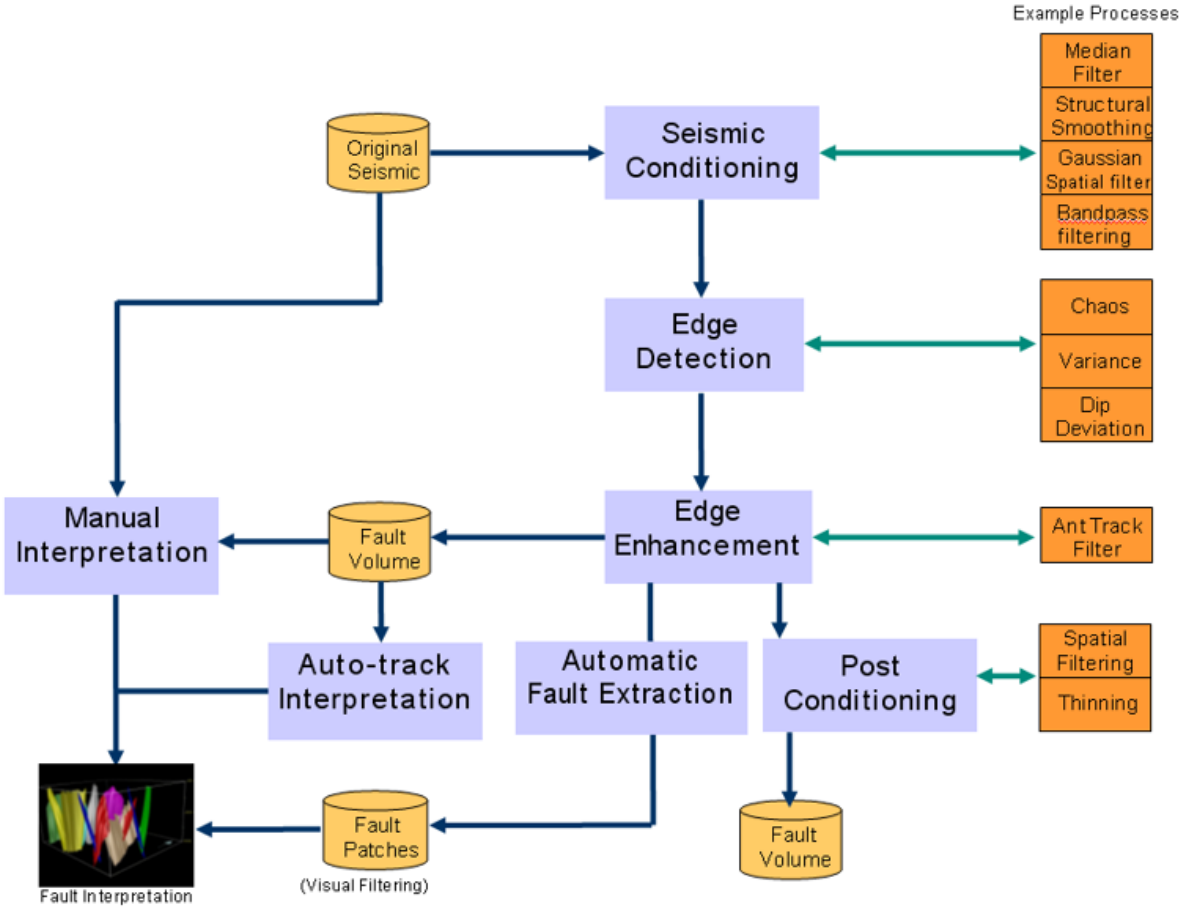


**Figure 6.** Schematic of ant tracking methodology (Ali et al., 2016).

c. Relative Impedance Acoustic Attributes (RAI)

Reservoir distribution in relative impedance acoustic attribute by Emujakporue & Enyenihi (2020) this attribute is used to describe sequence boundaries, and thickness variations. The acoustic impedance of a medium is given as:

$$I = \rho V \qquad (7)$$

where,

V : velocity (m/s)
I : acoustic impedance (kg/m$^2$s)
$\rho$ : density (kg/m$^3$)

High relative acoustic impedance values are associated with shale-bearing facies, while lower values are associated with sand intervals (Emujakporue & Enyenihi, 2020).

d. Sum of Negative Amplitude attribute

The sum negative amplitude attribute can be calculated by summing the negative

amplitudes shown in the following equation (Alamsyah, et al., 2023).

$$SNA = \sum_{i=1}^{N}(-a_i)N \quad (8)$$

Where, $a_i$ is the i-th amplitude value, with i=1,2,3, etc., and N is the number of negative amplitudes.

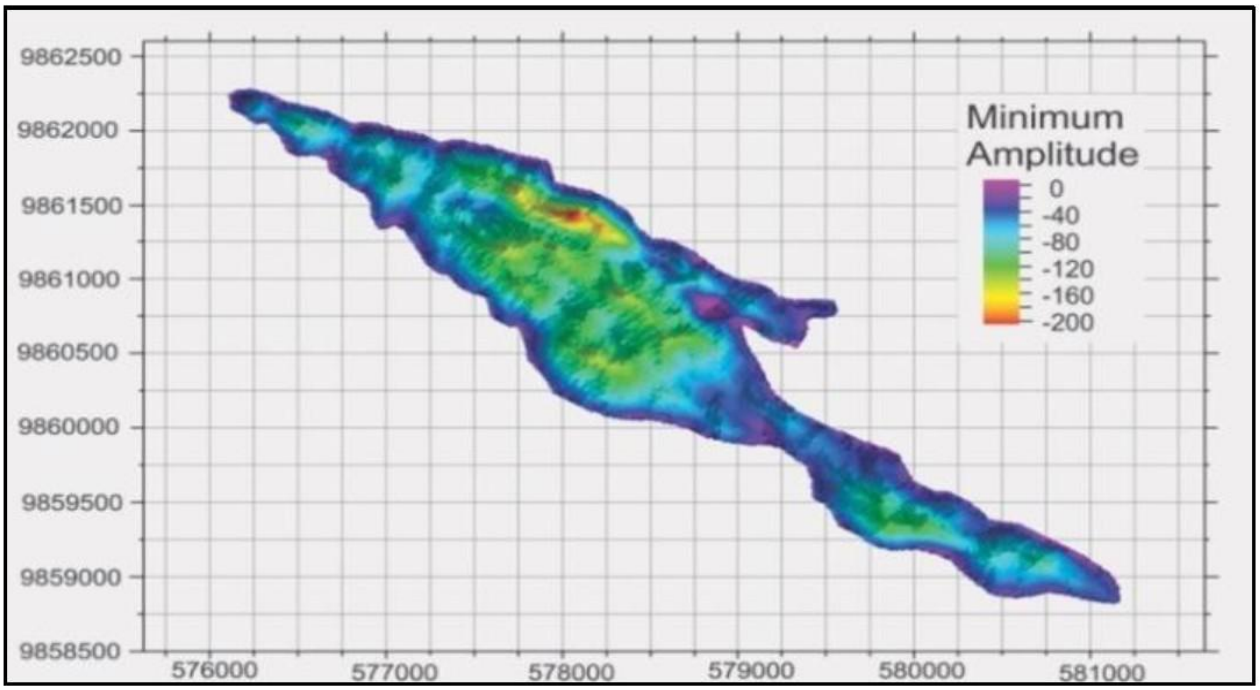


**Figure 7**. Example of minimum amplitude attribute application (Haris et al., 2018).

e. Minimum Amplitude Attribute

The minimum amplitude attribute calculates the minimum value of the trough or its minimum amplitude. This attribute in Haris et al. (2018) is used to see the distribution that shows the channel geometry of the sand body, which is obtained by extracting the tuning amplitude from the target reservoir surface area. The tuning amplitude illustrates that the channel sand body forms an elongated cluster and develops in a northwest to southeast direction as shown in Figure 7.

The sum of negative amplitude attribute results from the summation of negative values within the upper and lower analysis window coverage of the interest zone in the seismic data, which can indicate the presence of sand reservoirs and the presence of gaseous hydrocarbons, provided that the hydrocarbon zone is characterized by low impedance which is identical to the presence of through in the seismic cross section (Didi et al., 2022; Côrte et al., 2020; Okeke et al., 2021 and Hesham, et al., 2023). The relative acoustic impedance attribute is based on comparing the contrast between the reservoir impedance and the surrounding lithology in a particular interval. This attribute is widely used to delineate sequence boundaries, areas of unconformity and discontinuity, and the presence of fluid in the reservoir (Emujakporue & Enyenihi, 2020; Lohitanon, 2021; Allo et al., 2022; Franklin et al., 2023).

## Results and Discussion

*Multiattribute Analysis*

Multiattribute analysis was applied to 53 wells to predict logs because these wells did not have complete S-Wave logs.

The list of available attributes is shown in the right-side of Figure 8. Looking at the error trends in training and validation shows that log prediction only uses 4 attributes because the 5th attribute is

overtrained which is shown by the increasing validation error value. This is shown in left-side.

The predicted log S-wave output is shown in Figure 9. Multiattribute analysis was performed with inputs from wells RPH-16 and RPH-7 that had the originals S-Wave to predict the S-wave in wells RPH-8 and RPH-5. The correlation is 0.9, which indicates a good correlation of the multiattribute analysis result. Based on the result of overall multiattribute analysis on 57 wells, the S-wave log prediction results show a good correlation value of ≥ 0,86.

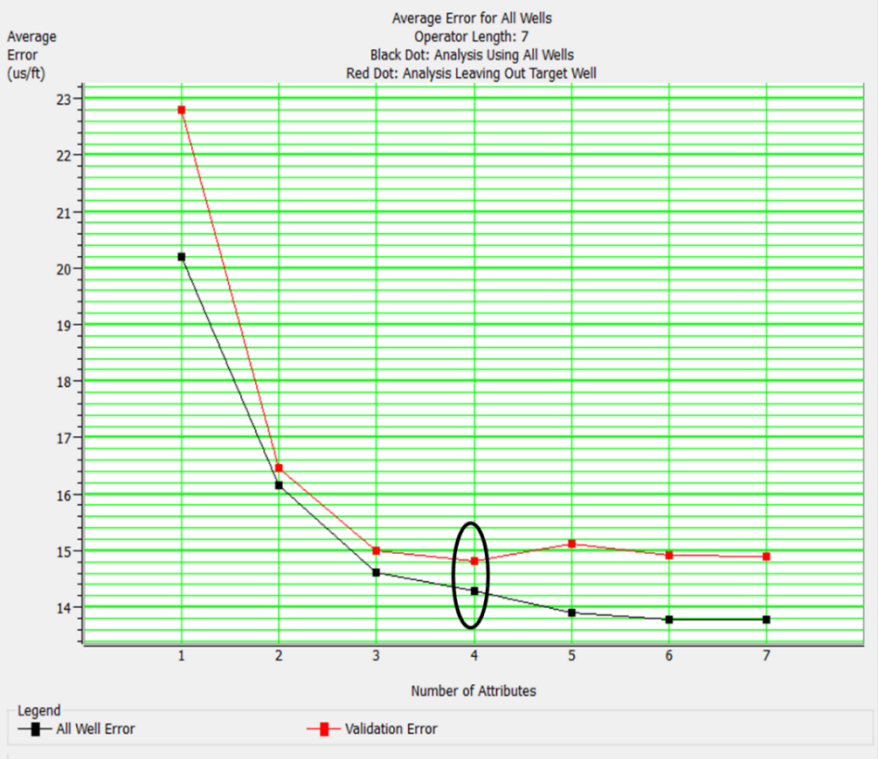


Multiple Attribute Correlation Results

Multi-Attribute List: Multi Attribute List 1

| | Target | Final Attribute | Training Error | Validatior |
|---|---|---|---|---|
| 1 | Sqrt( S-wave ) | Sqrt( Neutron Porosity ) | 20.226909 | 22.816695 |
| 2 | Sqrt( S-wave ) | Log( P-wave ) | 16.176267 | 16.476597 |
| 3 | Sqrt( S-wave ) | ( Gamma Ray )**2 | 14.631167 | 15.025293 |
| 4 | Sqrt( S-wave ) | Sqrt( Density ) | 14.309914 | 14.838132 |
| 5 | Sqrt( S-wave ) | Log( Resistivity ) | 13.914447 | 15.144828 |
| 6 | Sqrt( S-wave ) | Sqrt( Porosity ) | 13.808217 | 14.929293 |
| 7 | Sqrt( S-wave ) | Sqrt( Permeability ) | 13.802008 | 14.917780 |

**Figure 8.** (Bottom) List of available attributes for predicting Log S-Wave and (top) is error plot for each attribute showing the 4th best attribute.

*Sensitivity Analysis*

This analysis is divided into 3 which aims to separate the reservoir and non-reservoir zones using as in Figure 10, to separate the fluid filled reservoir zone and non-reservoir as in Figure 11, and then to discriminate the fluid that fills the reservoir as in Figure 13.

The results obtained for the reservoir zone have a P-Impedance value of 6000-9000 ((m/s)(g/cc)) which is in the range of P-impedance values of non-reservoir zones so that the P-impedance parameter in this case is less sensitive. While the Vp/Vs ratio of the reservoir zone is 1.1-1.5 which shows a smaller value than the non-reservoir zone.

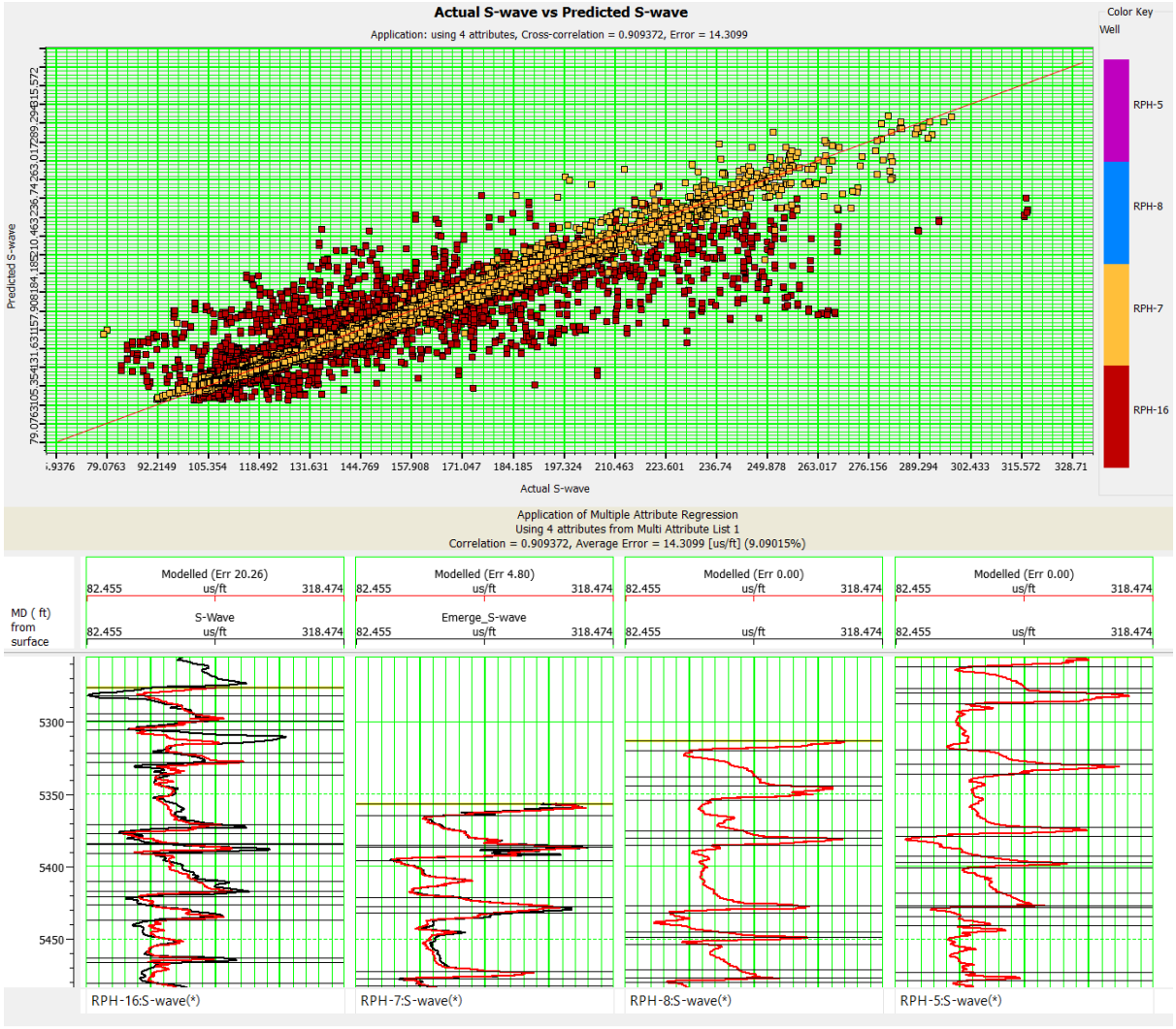


**Figure 9.** (top) Results showing correlation values and (bottom) comparison between original log S-wave (black) and predicted s-wave (red).

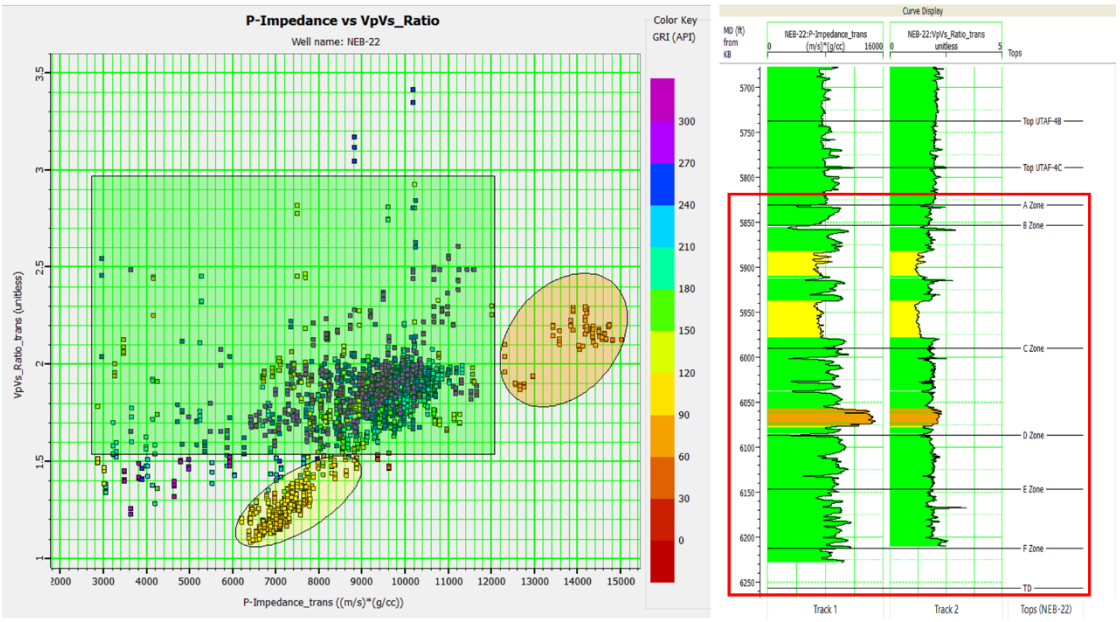


**Figure 10.** Sensitivity analysis to distinguish reservoir (yellow circle) and non-reservoir (green square).

In Figure 10, color-key gamma ray shows the difference in radioactive values contained in rocks so that rocks that are potentially reservoirs indicate lower gamma ray values because they have less radioactive content, this is shown in the yellow circle with a range of 60-100 (API). Non reservoir zones are indicated by higher gamma ray values marked with a green square.

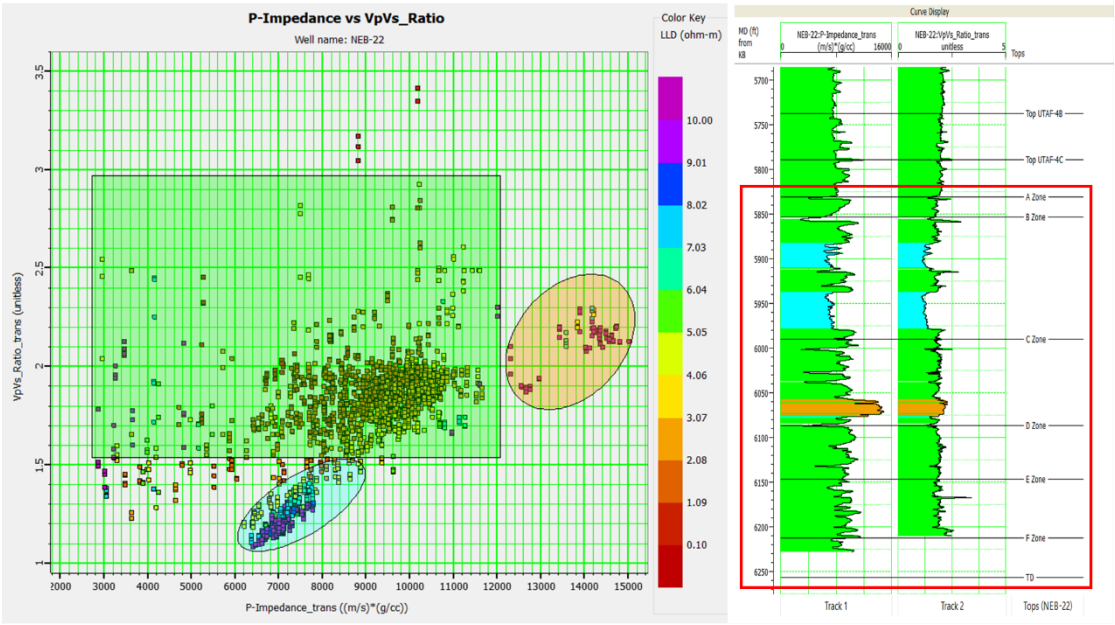


**Figure 11**. Sensitivity analysis to reservoir zones distinguishes fluid-filled (light blue circle) and non-reservoir.

In Figure 11, color-key resistivity indicates a permeable zone when it has a high resistivity value. When the reservoir is filled with hydrocarbons, the resistivity shows a higher value than when filled with water, this is shown in the light blue zone when filled with hydrocarbons, the resistivity is shown in red color with a value of 8-10 Ωm.

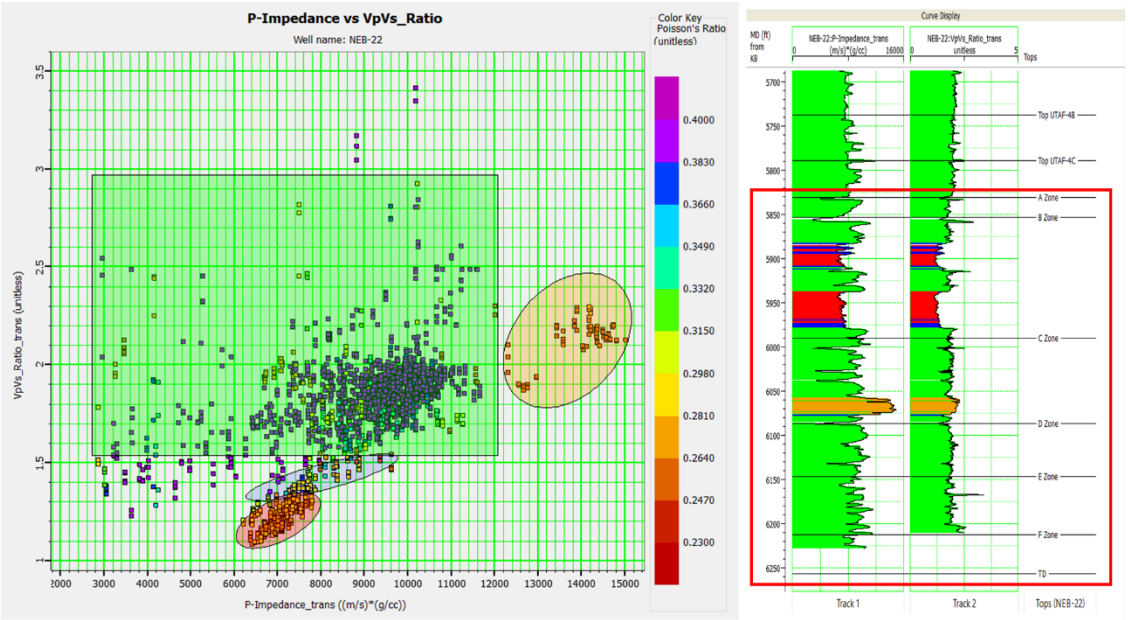


**Figure 12.** Sensitivity analysis to distinguish the type of fluid filling the reservoir (gas, oil, or water), but this figure shows the reservoir is only filled with gas (red circle) and water (blue circle).

In Figure 12, color-key Poisson's ratio indicates the type of fluid that fills the reservoir so that when filled by gas it will show a value of 0.1-0.25 marked with a red zone in curve display and when filled by water it will show a Poisson's ratio of 0.3 marked with a blue zone and non-reservoirs show a value > 0.3.

*Seismic Attribute Analysis*

Seismic attributes were applied to see the distribution of faults and reservoirs in area 'X'. Attribute values close to 1 are interpreted as the presence of faults, so the main faults in area 'X' are oriented north-south, northwest-southeast, and northeast-southwest (Figure 13). The higher fault intensity is in the eastern field area. While the lower fault intensity is in the western field area.

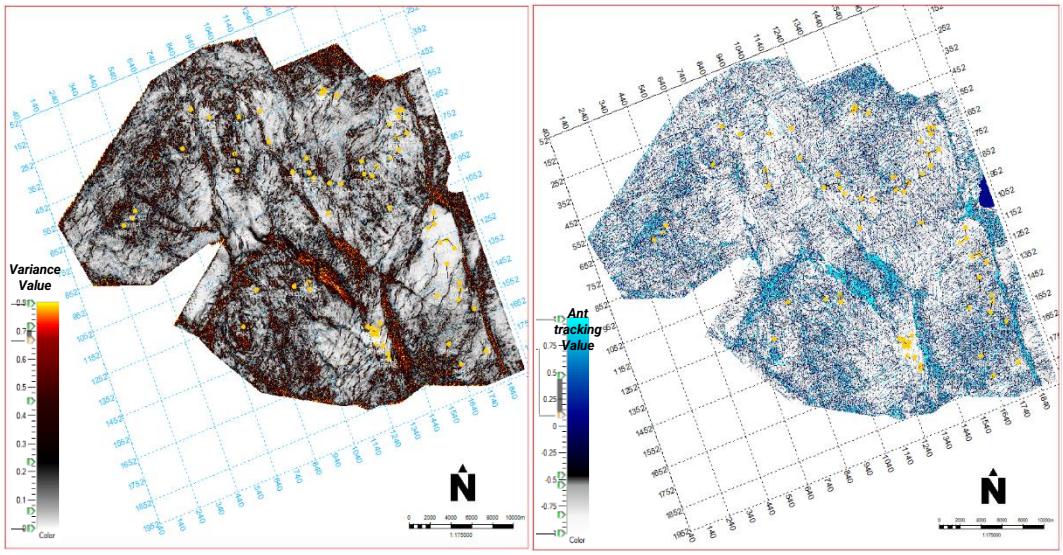


**Figure 13.** Visualization of intensity and distribution of faults in the LTAF Formation (right) Variance attribute, (left) Ant Tracking attribute.

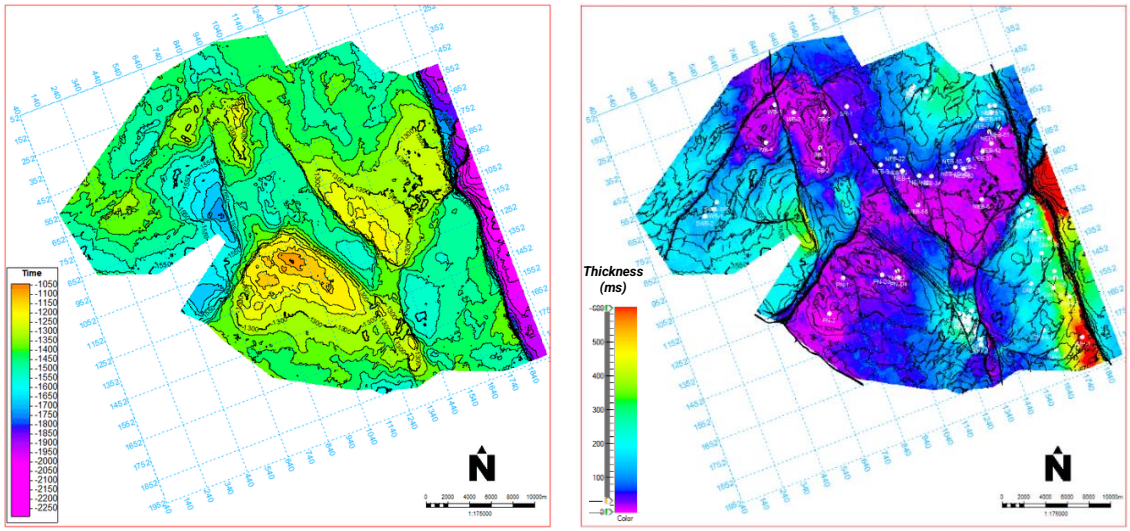


**Figure 14.** Relative thickness of reservoir (a) time structure map of LTAF Formation, (b) isochrone map of LTAF-Basement interval.

The relative thickness of the reservoir can be seen Figure 14. There is a time difference in the time structure indicating that shallower areas are shown with faster times, and vice versa. As for the relative thickness of reservoirs, it is indicated by dark blue-purple color with values <100 ms spreading in the center of area 'X', and thicker reservoirs are indicated by values >100 ms.

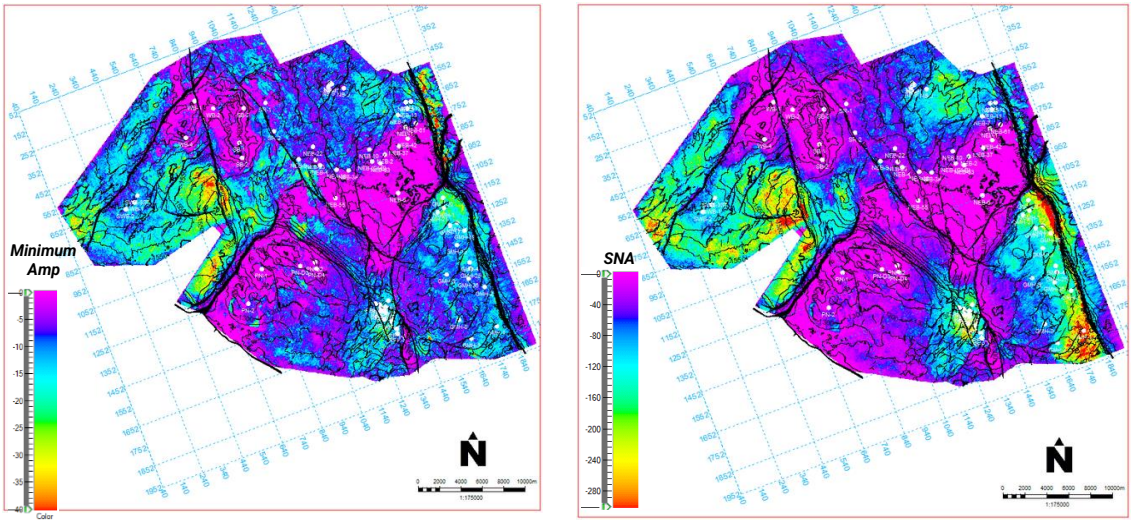


**Figure 15**. Reservoir distribution (a) Relative Acoustic Impedance-Minimum Amplitude attributes, (b) Sum of Negative Amplitude attributes.

Reservoir distribution is done by applying relative seismic data, namely Acoustic Impedance at the minimum amplitude attribute and conventional seismic at the Sum Negative Amplitude attribute.

So that the results obtained look consistent in describing the distribution of reservoirs shown in Figure 15. Attributes with low values are shown in purple, interpreted as areas that have higher porosity that spread in the middle of the area. Otherwise, research areas with relatively thick reservoirs are interpreted as having low porosity that spreads to the north, south, west, and southeast shown in light blue to red.

*Distribution of $CO_2$ Impurities*

The percentage of natural $CO_2$ distribution was obtained from well test data. The data shows the $CO_2$ content contained in the hydrocarbons in each well, which is then mapped to the natural $CO_2$ saturation distribution. Yellow to red colors indicate high saturation of impurities with a percentage of >50%, while purple indicates low saturation with a percentage of <50%. The distribution of high $CO_2$ saturation spreads in the eastern part. While the distribution of low $CO_2$ saturation spreads in the western part of the 'X' area. The areas with high and low impurity saturation are separated by a large northwest-southeast trending fault. Towards the west, the $CO_2$ saturation spreads with a low percentage. The high $CO_2$ impurity originates from the Betara Deep area associated with the pre-tertiary basement and the high intensity of faults and fractures in the area that affect the hydrocarbon distribution.

Integration of the LTAF and Isochron structure maps (Figure 16) with the seismic result map of the sum of negative amplitude and relative impedance attributes to identify the gross distribution of sandstone reservoirs in the LTAF interval regionally shows the same trend. The trend of reservoir distribution shows N-S and NE-SW directions, which correspond to the regional trend distribution map of LTAF sedimentation described in Figure 1. In general, the sandstone reservoirs in this LTAF interval have low-impedance elastic parameters (Alamsyah, 2010) and thus show negative valuations in seismic amplitude (Alamsyah et al., 2023). Qualitatively, integrating these maps is a good validation to describe the gross distribution of sandstone reservoirs for the LTAF interval in this X area.

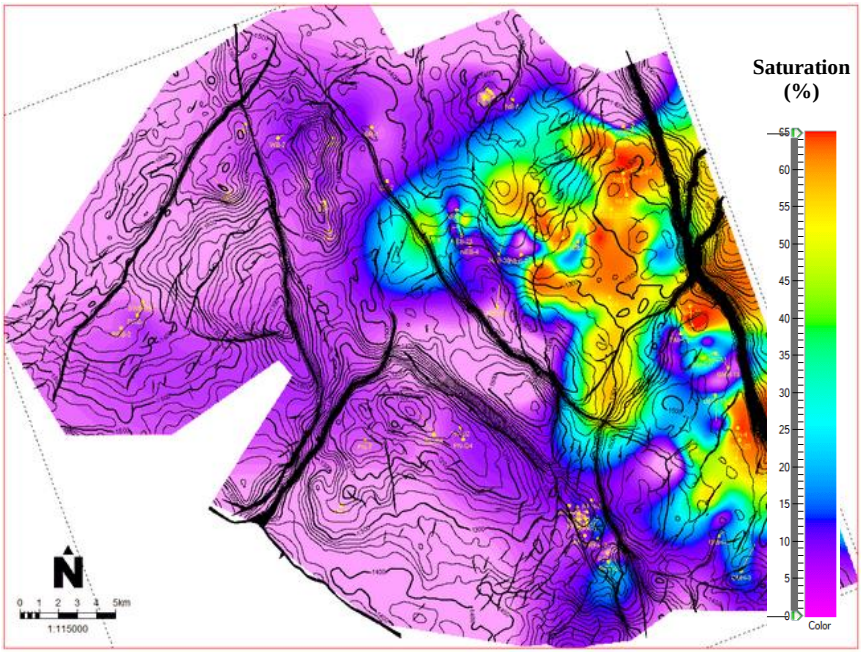


**Figure 16.** Saturation distribution map of natural $CO_2$ impurities (well based) in the LTAF-Basement interval which shows high in the eastern area.

From the attribute model, the consistency is shown by the significant intensity in the area adjacent to the main fault zone, which is oriented N-S and NE-SW. This significant intensity may result from the reactivation of the main faults during the inversion process so that it can be an alternative migration path for hydrocarbons to fill the reservoir in the LTAF interval. The integration results show the correspondence between the distribution of $CO_2$ saturation and the intensity of fractures and faults, where the high $CO_2$ saturation comes from the east with a reasonably high $CO_2$ saturation, and the further west, the $CO_2$ saturation decreases. There is consistency in the distribution of sandstone reservoirs based on the resulting seismic attributes, and the intensity of fractures and faults also affects the $CO_2$ migration path.

The results of this study provide information and validation for the western region of Area X, which has the potential for field development with thick reservoir zones and low $CO_2$ impurities content. This potential area must be followed up with reservoir engineering studies and its subsurface and non-subsurface economics.

## Conclusion

The study concludes that sandstone and hydrocarbon reservoirs in the LTAF interval of area X are primarily sensitive to elastic P-Impedance and Vp/Vs ratio. In contrast, sandstone reservoirs are characterized by low impedance and gas hydrocarbons by a low Vp/Vs ratio. In Area X, the fault distribution trends north-south, northwest-southeast, and northeast-southwest, with a higher intensity in the eastern section, while relatively thick reservoirs are distributed across the north, south, west, and southeast. The distribution of $CO_2$ impurity saturation gets lower towards the west. With the consistency of the distribution of $CO_2$ impurity saturation to reservoirs and the intensity of faults and fractures obtained from seismic attribute analysis, it is possible to identify areas with thick reservoirs and low $CO_2$ zones that have the potential for further development.

## Acknowledgements

The authors would like to thank PT PetroChina International Jabung Ltd. for providing secondary data that supports this research.

**Author Contribution**

Authors 1 and 3 discuss, interpret and write the script, authors 2 4 and 5 discuss and assist in proofreading the script.

**Conflict of Interest**

The authors declare no conflict of interest.

**References**

Abdel-Fattah, M. I., Pigott, J. D., & El-Sadek, M. S. (2020). Integrated Seismic Attributes and Stochastic Inversion for Reservoir Characterization: Insights from Wadi Field (NE AbuGharadig Basin, Egypt). *Journal of African Earth Sciences*, 161, 103661. https://doi.org/10.1016/j.jafrearsci.2019.103661

Alamsyah, M. N., Fitrianto, T., Sukmono, S., & Winardhi, S. (2023). A Preliminary Analysis of Natural $CO_2$-Saturated Gas Sands Distribution in the Gemah Field-Jabung Block, South Sumatra Basin, Indonesia, by using Simple Seismic Attributes. *The Leading Edge*, 42(11), 726-788. https://doi.org/10.1190/tle42110748.1

Alamsyah, M. N., & Muhtar, L. K. (2017). AVA Characteristics on Alluvial Facies Reservoir - Case Study : NEB Field, Jabung Block, South Sumatera Basin. *Conference paper* https://www.researchgate.net/publication/346974001

Allo, O. J., Bako, M. E., & Esan, D. (2022). Seismic Attribute Analysis for Prospect Delineation in 'TMB' Field, Niger Delta Basin, Nigerial. *Journal of Applied Sciences and Environmental Management*, 26(3), 487–494. https://doi.org/10.4314/jasem.v26i3.17

Ambarsari, D. S., Winardhi, I. S., Prakoso, S., & Sukmono, S. (2020). Reservoir quality determination by using critical porosity and volume of clay: A case study in the Talang Akar Formation in the NW Java Basin, Indonesia. *First Break*, 38(5), 63–70. https://doi.org/10.3997/1365-2397.fb2020035

Côrte, G., Dramsch, J., Amini, H., & MacBeth, C. (2020). Deep Neural Network Application for 4D Seismic Inversion to Changes in Pressure and Saturation: Optimizing the use of Synthetic Training datasets. *Geophysical Prospecting*, 68(7), 2164–2185. https://doi.org/10.1111/1365-2478.12982

Didi, C. N., Obiadi, I. I., Okeke, S. E., Anakor, S. N., & Ikomi, M. K. (2022). Lithostratigraphic Interpretation and The Analysis of The Depositional Environment of Nigeria Chad Basin using Well Log Data and Seismic Data. *Meridian Journal of Physical Sciences*, 2(1), 70–112. https://www.theinterscholar.org/journals/index.php/mjps/article/view/164

Emujakporue, G. O., & Enyenihi, E. E. (2020). Identification of Seismic Attributes for Hydrocarbon Prospecting of Akos Field, Niger Delta, Nigeria. *SN Applied Sciences*, 2(5), 910. https://doi.org/10.1007/s42452-020-2570-1

Franklin, E. C., Ndubuisi, E. G., & Udoka, C. I. (2023). Reservoir identification in Bornu Basin, Northeastern Nigeria using seismic attribute analysis. *International Journal of Scientific Research in Multidisciplinary Studies*, 9(2), 01–08. https://www.isroset.org/journal/IJS

RMS/full_paper_view.php?paper_id=3064

Ginger, D., & Fielding, K. (2005). The Petroleum Systems and Future Potential of The South Sumatra Basin. *Proc. Indon Petrol. Assoc., 30th Ann. Conv.* Thirtieth Annual Convention. https://doi.org/10.29118/IPA.2226.05.G.039

Haris, A., Riyanto, A., & Mardiyati, S. (2018). Statistical Tuning Chart for Mapping Porosity Thickness: A Case Study of Channel Sand Bodies in the Kutei Basin Reservoir. *TELKOMNIKA(Telecommunication Computing Electronics and Control)*, 16(6), 2676–2682. https://doi.org/10.12928/telkomnika.v16i6.9660

Hesham, A., Fattah, N. A., & Dahroug. A. (2023). Integrating Seismic Attributes and Rock Physics for Delineating Pliocene Reservoir in Disouq Field, Nile Delta, Egypt. *Contributions to Geophysics and Geodesy*, 53(1), 65–84. https://doi.org/10.31577/congeo.2023.53.1.4

Hidayat, M., Hartanto, D. T., Azis, M. M., & Sutijan, S. (2020). Studi Penambahan Etilena Glikol dalam Menghambat Pembentukan Metana Hidrat pada Proses Pemurnian Gas Alam. *Jurnal Rekayasa Proses*, 14(2), 198–212. https://doi.org/10.22146/jsrekpros.59871

Hijria, T. V., & Danusaputro, H. (2016). Analisis Persebaran Zona Reservoir Lapangan DT-1 Menggunakan Metode Inversi Impedansi Akustik dan Atribut Variansi. *Youngster Physics Journal*, 5, 1–12. https://ejournal3.undip.ac.id/index.php/bfd/article/view/10627

Lohitanon, P. (2021). Reservoir imaging using seismic attributes, Pattani Basin, Thailand. *Bulletin of Earth Sciences of Thailand*, 10(2), 142–152. https://ph01.tci-thaijo.org/index.php/bestjournal/article/view/246753

Ngeri, A. P., Tamurnobereton-ari, I., & Amakiri, A. (2015). Ant-tracker attributes: An Effective Approach to Enhancing Fault Identification and Interpretation. *IOSR Journal of VLSI and Signal Processing*, 5(6), 67–73. https://www.iosrjournals.org/iosr-jvlsi/papers/vol5-issue6/Version-2/J05626773.pdf

Okeke, S., Didi, C., Ngene, T., & Oyekola, P. (2021). Evaluation of Prospective Hydrocarbon Zones in Soedinc Field, Offshore Norway. *11th Annual International Conference on Industrial Engineering and Operations Management*, IEOM Society International. http://dx.doi.org/10.46254/AN11.20211076

Ali, A., Othman, A., Mohamed, A. A. M., & Mohamed, F. M. (2016). Improving Fault Tracing Detection Applying 3D Ant Tracking Seismic Attribute. *IOSR Journal of Applied Geology and Geophysics*, 4(3), 18–25. https://www.iosrjournals.org/iosr-jagg/papers/vol4-issue3/Version-1/D0403011825.pdf

Pratama, E., Mulyatno, B. S., & Zaenudin, A. (2019). Analisis Reservoar Migas (Sandstone) Menggunakan Multiatribut Seismik pada Lapangan TG12, Cekungan Barito, Kalimantan Selatan. *Jurnal Geofisika Eksplorasi*, 5(1), 3–14. https://doi.org/10.23960/jge.v5i1.19

Russell, B. (2015). Visualizing Inversion Results with Rock Physics Templates. *CREWES Research Report*, *Volume 27*.

Russell, Hampson. (2017). *CGG GeoSoftware Log Transform Theory*. HRS.

Sanjaya, A. S., & Nofendy, A. (2018). Prediksi Pembentukan Hidrat Gas dengan Pengaruh Joule-Thomson Effect yang Diakibatkan oleh Choke Performance. *Jurnal Chemurgy*, 1(1), 1–8. https://doi.org/10.30872/cmg.v1i1.1132

Sembiring, S., Panjaitan, R. L., Susianto, S., & Altway, A. (2019). Pemanfaatan Gas Alam sebagai LPG (*Liquified Petroleum Gas*). Jurnal Teknik ITS, 8(2), F206–F211. https://doi.org/10.12962/j23373539.v8i2.47079